Modeling and Design Analysis of a Permanent Magnet Linear Synchronous Generator

Technical Report UIUC-ESDL-2013-01*

Xin Niu†
Engineering System Design Lab
University of Illinois at Urbana-Champaign

August 25, 2013

Abstract

Ocean wave energy conversion is a popular research area due to the increasing scarceness of nonrenewable energy resources. However, extracting wave energy is not a simple process. For example, the design and construction of wave energy take-off devices that are reliable, long-lasting, and efficient is a non-trivial endeavor. In this report, the physics-based theories behind a permanent magnet linear generator are reviewed. A model of the generator is built from a series of independent and dependent parameters. The model is simulated using MATLAB® with a specific set of parameter values. Two of the independent parameters are studied and improvement potential is revealed.

*This technical report was submitted in partial fulfillment of an independent study project at the University of Illinois at Urbana-Champaign Department of Industrial and Enterprise Systems Engineering.

†B.S. Candidate in Industrial Engineering, Department of Industrial and Enterprise Systems Engineering, University of Illinois at Urbana-Champaign, xinniu2@illinois.edu.

Contents

1 Permanent Magnet Linear Synchronous Generators

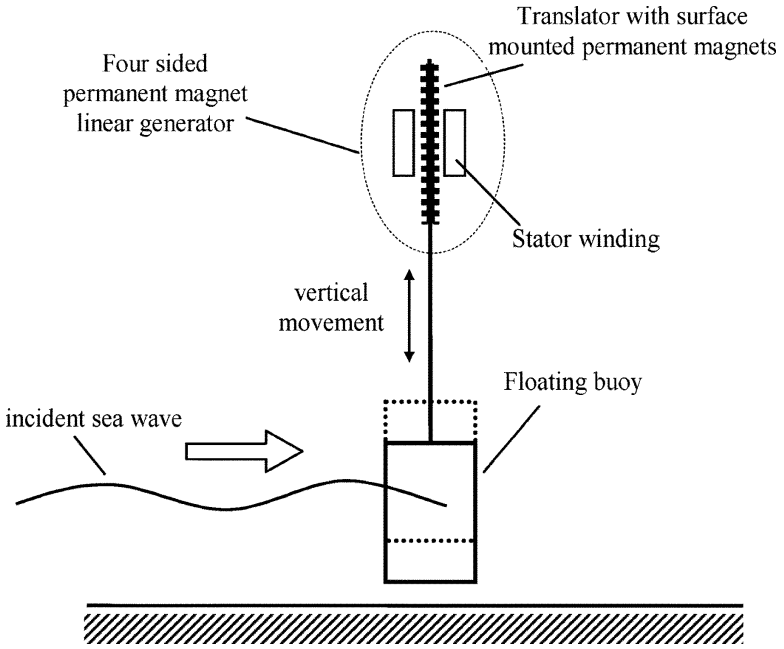

Figure 1: Heaving Linear Generator Power Take-Off Device for Wave Energy Conversion (from Ref. [1]).

This report describes a model for a permanent magnet (PM) linear synchronous generator that is part of a system for converting ocean wave energy into electricity [2]. A dynamic mathematical model of such a generator was developed based on Ref. [2], and tested using a variety of simulations. A generator is known as "synchronous" when the waveform of the generated voltage is synchronized with the rotation of the generator. Permanent magnets are used to provide the field excitation in a linear synchronous generator. Due to mechanical constraints, linear motors have large and variable airgaps [3]. Therefore, the magnetic circuit has a large reluctance. Magnetic reluctance, or magnetic resistance, is a property of magnetic circuits. The concept of magnetic reluctance is analogous to resistance in an electrical circuit. However, instead of dissipating electrical energy, magnetic reluctance stores magnetic energy. An electric field causes an electric current to follow the path of least resistance. Similarly, a magnetic field causes magnetic flux to follow the path of least magnetic reluctance. A permanent magnet linear synchronous motor requires magnets with a large coercive force, which is the intensity of the applied magnetic field required to reduce the magnetization of that material to zero after the magnetization of the material has been driven to saturation. When a material has a large coercive

force it is difficult for the material to lose its magnetization. Using magnets with a large coercive force results in a permanent magnet generator that has stable properties over time. Ferrite and rare-earth magnets are examples of permanent magnets with a large coercive force [3].

1.1 Electromagnetic Theory

Pertinent elements of electromagnetic theory will be reviewed here as a foundation for understanding the operation of permanent magnet linear synchronous generators. For a circuit carrying a current I as shown in Fig. 2, the magnetic field intensity H at a point P is defined by the following equation:

$$\boldsymbol{H} = \frac{1}{4\pi} I \int_C \frac{d\boldsymbol{l} \times \boldsymbol{r_1}}{r^2}. \tag{1.1}$$

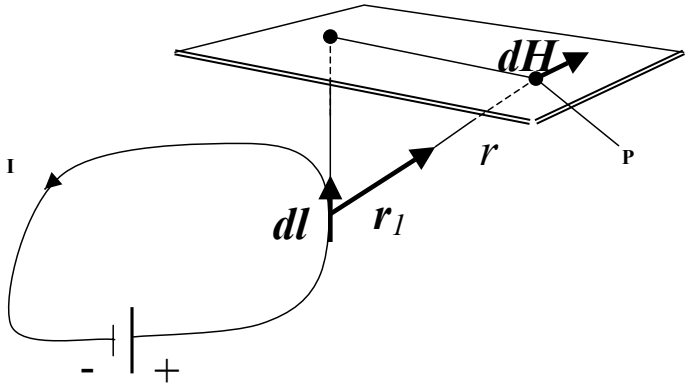

Figure 2: The Magnetic Intensity $d\boldsymbol{H}$ Produced by a Line Element $d\boldsymbol{l}$ of the Current I in a Circuit (from Ref. [4]).

The integration is carried out over a closed circuit C. The unit vector $\mathbf{r}_1$ and the distance r show the direction and distance respectively from the source to the point of observation. Magnetic field intensity is expressed in amperes per meter (A/m).

A magnetic field B is quantified by the force that it exerts on a conductor carrying an electrical current. It is related with the magnetic field intensity as follows:

$$\boldsymbol{B} = \mu \boldsymbol{H}, \tag{1.2}$$

where the constant μ is the permeability of the medium the magnetic field passes through. Magnetic field is expressed in Tesla (T or $\mathrm{N \cdot A^{-1} \cdot m^{-1}}$). If the material

is nonlinear, the permeability is a function of $\boldsymbol{B}$:

$$\mu = \frac{\boldsymbol{B}}{H(\boldsymbol{B})}. \tag{1.3}$$

The permeability of free space μ_0 is defined as: $\mu_0 = 4\pi \times 10^{-7}$ T $\cdot$ m/A.

The magnetic flux through a surface S is the component of the magnetic field $\boldsymbol{B}$ passing through that surface:

$$\Phi = \int_S \boldsymbol{B} \cdot d\boldsymbol{A}, \tag{1.4}$$

and is measured in Weber (W or T $\cdot$ m^2).

The magnetization $\boldsymbol{M}$ is the magnetic moment per unit volume at a given point in a medium. The magnetic moment is associated with the orbital and spinning motion of electrons. It has the same unit as the magnetic field intensity, A/m. When magnetization $\boldsymbol{M}$ is present, it combines with the magnetic field intensity $\boldsymbol{H}$ to produce the magnetic induction through the field equation:

$$\boldsymbol{B} = \mu_0(\boldsymbol{H} + \boldsymbol{M}). \tag{1.5}$$

The fundamentals of a permanent magnet linear synchronous generator are closely related to magnetic field and Maxwell equations. Three of the four equations are related to permanent magnet linear synchronous generators by Ampere's Law:

$$\nabla \times \boldsymbol{H} = \boldsymbol{J} + \frac{\partial \boldsymbol{D}}{\partial t}. \tag{1.6}$$

Here $\boldsymbol{J}$ is the volume current density in the circuit. The second term ($\partial D/\partial t$) involves electric displacement $\boldsymbol{D}$, which is a vector field that accounts for the effects of free charge within materials. When the cyclic variation of $\boldsymbol{D}$ has low frequency, which is the case in this report, the second term is considerably smaller than $\boldsymbol{J}$. Therefore, electric displacement will be neglected in this report. With this simplification, Eqn. (1.6) can be rewritten as follows:

$$\oint_C \boldsymbol{H} \cdot d\boldsymbol{l} = \int_S \boldsymbol{J} \cdot d\boldsymbol{A}. \tag{1.7}$$

Equation (1.7) states that line integral of $\boldsymbol{H}$ over a closed curve C is equal to the current crossing the surface S bounded by C. Often the same current crosses the surface bounded by the curve C several times. A solenoid is a coil wounded into a tightly packed helix, as illustrated in Fig. 3. A current runs through the coil and creates a magnetic field. With a solenoid, C could follow the axis and then return outside the solenoid. The total current crossing the surface is then the current in each turn multiplied by the number of turns. Equation (1.7) describes how the magnetic field intensity is determined by the distribution of current in a circuit. This equation governs the behavior of the stator part of a

permanent magnet linear synchronous generator. The stator is the stationary portion of the generator. It contains an electric circuit, and current is induced in the stator circuit by the moving permanent magnets located on the translator. The stator and translator are depicted in Fig. 1.

$$\nabla \times \boldsymbol{B} = 0. \tag{1.8}$$

Equation (1.8) is the second of the three Maxwell's equations discussed here, and is also known as Gausss law. It states that the net flux of $\boldsymbol{B}$ in any volume is zero. Unlike electrical field lines, a magnetic field line must complete a closed, continuous curve. This must always be taken in to account in the design of the magnetic circuit of a generator.

$$\nabla \times \boldsymbol{E} = -\frac{\partial \boldsymbol{B}}{\partial t}. \tag{1.9}$$

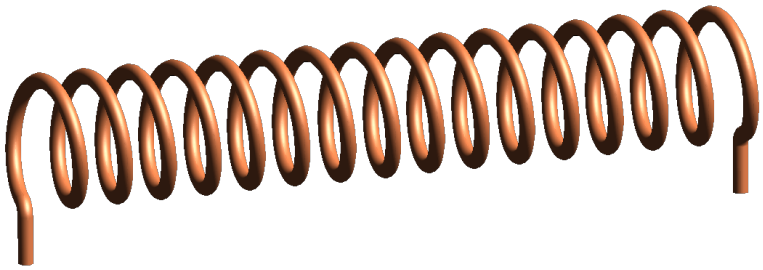

Figure 3: An Example of a Solenoid.

Equation (1.9) is the third of Maxwell's equations relevant to linear generators, and states that the curl of the electric field is equal to the negative time derivative of the magnetic field. This demonstrates the duality of electric and magnetic fields. In physics, in the static case, electromagnetism has two separate facets: electric fields and magnetic fields. This gives rise to the electromagnetic dual concept. Expressions of either of these will have a dual expression of the other. The reason behind this is related to special relativity when using Lorentz transformation to transform electric fields to magnetic fields. Some examples of the duality of electric and magnetic fields include electric field and magnetic field, electric displacement field and magnetizing field and Faraday's law and Ampere's law. Equation (1.9) can be rewritten by using Stokes Theorem on the left hand side and Eqn. (1.4) on the right hand side:

$$e = -\frac{d\Phi}{dt}, \tag{1.10}$$

where e is the electromotive force (EMF) and Φ is the magnetic flux through a closed surface.

Equation (1.10) is the most widespread formulation of Faraday's Law, which states: The induced electromotive force, which is the voltage generated, in any

closed circuit is equal to the negative of the time rate of change of the magnetic flux through the circuit. The direction of the current induced in the circuit is such that its magnetic field opposes, to a greater or lesser extent depending on the resistance of the circuit, the change in flux. If the closed circuit comprises N turns close together, each intercepting the same magnetic flux, then the electromotive forces add up, resulting in an N times larger electromotance. With this in mind, we can define $N\Phi$ as the flux linkage Λ:

$$\Lambda = N\Phi, \tag{1.11}$$

and Faraday's Law for circuits with multiple turns can be rewritten as:

$$e = -\frac{d\Lambda}{dt}. \tag{1.12}$$

2 Dynamic System Model

There are two primary types of permanent magnet linear synchronous generators: tubular permanent magnet linear synchronous generators and flat permanent magnet linear synchronous generators. The tubular permanent magnet linear synchronous generator is cylindrical. The force-to-weight ratio of such machines has been proved to be higher than flat generators [5]. However, flat generators are less expensive and easier to build.

In this report two models of a permanent magnet linear synchronous generator will be built and simulated. A series of differential equations will be formulated to describe the incident ocean wave and the reaction of the permanent magnet linear synchronous generator. The incoming ocean wave is assumed to be sinusoidal. For the first model, we ignore the reaction force applied by the generator. The second model includes the effect of the reaction force of the generator. These two models were then used to simulate dynamic generator behavior. Generator performance was evaluated using each model.

2.1 System Description

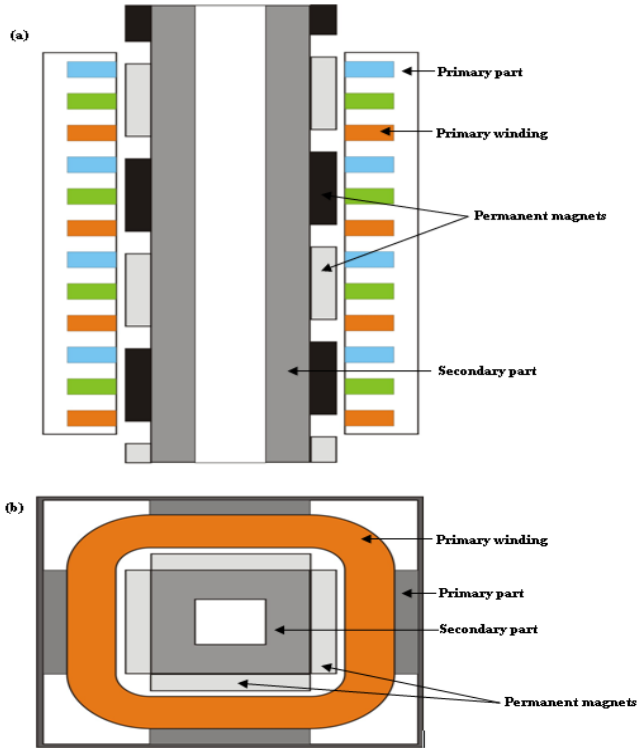

Figure 4: Schematic of the Quasi-Flat Tubular Permanent Magnet Linear Synchronous Generator: **(a)** Longitudinal Cross-Section **(b)** Top-View (from Ref. [2]).

The proposed structure of the permanent magnet linear synchronous generator is shown schematically in Fig. 4, which is based on the structure from Ref. [2]. It consists of four flat primary elements and four secondary elements enclosed within one housing. The secondary elements, which correspond to the translator in Fig. 1, move with the buoy and are called translators, which are the non-stationary parts in a generator. The primary elements, which correspond to the stator winding in Fig. 1, don't move and are called stators. Each of the flat sides is similar in structure to a flat linear machine as shown in Fig. 5.

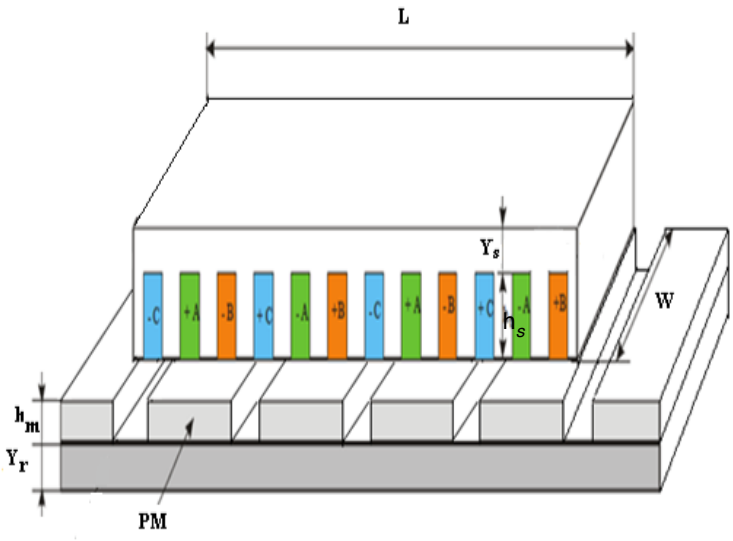

Figure 5: Structure of the Flat Permanent Magnet Linear Synchronous Generator (from Ref. [2]).

Figure 5 depicts the stator, which is the top element in the figure, and the translator, which is the bottom element shown in the figure. The stator contains the windings. Normally a permanent magnet linear synchronous generator contains a number of individual windings stacked together. The model in this report describes a permanent magnet linear synchronous generator with three phases. The three phases of windings are labeled A, B, and C. L is the length of the stator core. Y_s is the stator yoke thickness. h_s is the height of the slot. W is the width of the stator. h_m is the height of the magnet. Y_r is the translator yoke thickness.

The translator will move along with the buoy that moves with the ocean wave. Since the magnets on the translator are also moving with it, the magnetic field that passes through the motionless stator windings will change with time. According to Faraday's Law discussed in the previous section, this will induce currents in the circuit. This is the mechanism that transforms the kinetic energy of the ocean wave into electricity. A dynamic model of this energy conversion based on differential equations will be presented later in this section.

2.2 Generator Model

The structure of the primary core is shown as below, where g_{eq} is the equivalent air gap. The primary core is the stator. The secondary core is the translator.

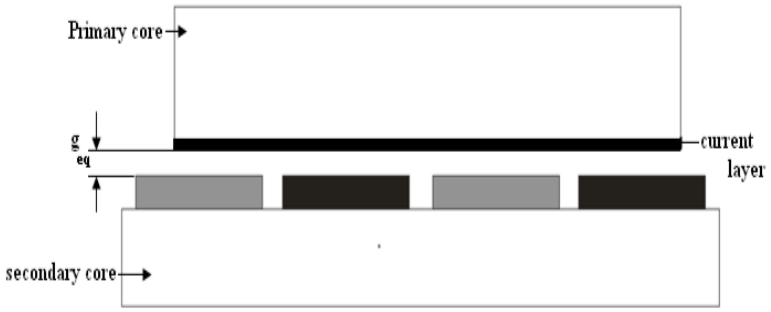

Figure 6: Schematic Representation of Unslotted Primary Core (from Ref. [2]).

The stator circuit windings run through slots in the stator. The slot dimensions are shown below:

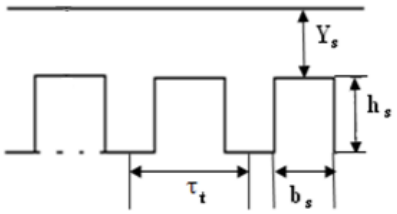

Figure 7: Illustration of Primary Core Slots (from Ref. [2]).

An equivalent circuit model of the generator is shown in Fig. 8:

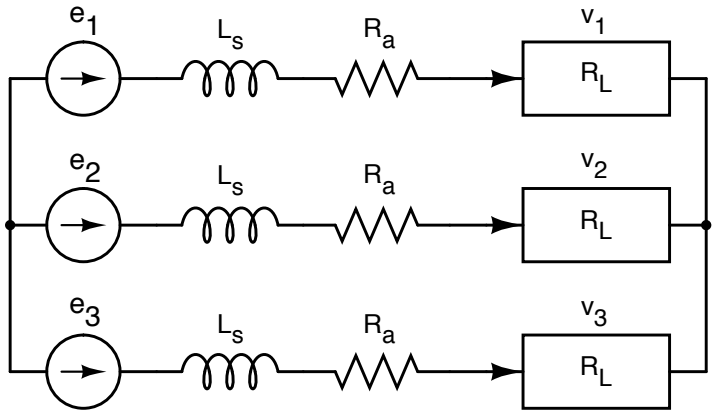

Figure 8: Equivalent Circuit of 3-Phase Winding of Generator (from Ref. [2]).

Table 1: Generator Parameters (from Ref. [2]).

Name	Symbol	Value	Units
Number of phases	m	3	
Number of poles	p	6	
Number of slots/pole/phase	q	1	
Number of armatures	M_s	4	
Number of turns per coil	N	82	
Length of the stator core	L	0.432	m
Stator width	W_s	0.2	m
Air gap	g_a	0.002	m
Height of magnets	h_m	0.006	m
Permissible flux density in translator core	B_r	1.2	T
Coercive magnetic field intensity	H_c	905000	A/m
Armature resistance	R_a	1.5	Ω
Load resistance	R_L	7.5	Ω
Synchronous inductance	L_s	0.115	H

Table 1 lists model parameters. The values used for most parameters listed in this table are based on the values given in Ref. [2]. Some parameters, namely m, p, q, M_s, N, L, W_s, g_a and h_m, are physical parameters and independent from each other. They are variables that can be changed by designers, and are treated as independent design variables in this report. However, it should be noted that they still have finite ranges of validity due to physical constraints. In addition, not all combinations of variable values within allowed ranges are physically meaningful. B_r and H_c are properties of the magnetic material used in Ref. [2].

We assume the magnetic material choice is fixed, so these two parameter values are not changeable here. Please note that some parameters, including R_a, R_L and L_s, are dependent parameters that will change with the physical design of the generator, but are considered to be fixed here for the specific generator design detailed in Ref. [2]. This assumption simplifies modeling, but does reduce model fidelity to some degree.

The number of turns per coil N refers to the number of turns in each of the three stator windings. The model in this report is a four-sided permanent magnet linear synchronous generator, with the windings on the stator elements. For the generator architecture used here, the stator elements are known also as armatures, which the power-producing component in a generator. Therefore this generator has four armatures, one for each side.

The armature resistance R_a is the resistance of each phase of the armature circuits. The synchronous inductance L_s is the inductance in each phase, and the load resistance R_L is the resistance of the load in the circuit. The load refers to an external electrical system being powered by the generator. These elements are depicted in the equivalent circuit model that is illustrated in Fig. 8.

The pole pitch τ_p is the overall width of each pole. It may be expressed as a function of stator core length L and the number of poles p:

$$\tau_p = \frac{L}{p}. \tag{2.1}$$

The tooth pitch τ_t may be derived from the pole pitch, and is illustrated in Fig. 7:

$$\tau_t = \frac{\tau_p}{mq}, \tag{2.2}$$

where m is the number of phases and q is the number of slots per phase per pole. Here we assume the slot width is:

$$b_s = 0.016 \text{ m}. \tag{2.3}$$

Knowing b_s, we can calculate tooth width:

$$b_t = \tau_t - b_s. \tag{2.4}$$

In a slotted armature, the effective area of the magnetic flux path is substantially reduced due to its geometry. This results in an increase in air gap reluctance. This phenomenon may be understood by studying Carter's coefficient (K_c) for air gap reluctance. In this simple method for estimating the air gap reluctance, we assume that the air gap flux is uniformly distributed over the whole of the slot pitch except for a fraction of slot width. This is possible because of how small the air gap is relative to the rest of the geometry (i.e., the stator is very close to the magnets). In fact, the magnetic field just above the magnet surface is perpendicular to the surface and uniform. Therefore, we can assume that the stator element is in this nearly uniform magnetic field.

Carter proposed a model for estimating air gap reluctance based on a coefficient that depends upon the ratio of slot width to gap length [6, 7]. In this approach we account for increased air gap reluctance by computing an equivalent air gap g_{eq}, which then influences flux density calculations. The equivalent air gap is calculated as follows:

$$g_{\text{eq}} = K_c \cdot g_a, \tag{2.5}$$

where Carter's Coefficient obtained by evaluating the following expression [2]:

$$K_c = \frac{\tau_t(5g_a + b_s)}{\tau_t(5g_a + b_s) - b_s^2}. \tag{2.6}$$

For each phase, the air-gap flux density (accounting for increased reluctance) is:

$$\phi = \frac{B_r h_m H_c \mu_0}{h_m H_c \mu_0 - g_{eq} B_r}. \tag{2.7}$$

The voltage equations associated with the equivalent circuit in Fig. 8 are as follows, where $e_{1,2,3}$ are the values of induced electromotive force for each phase:

$$e_1 = R_a i_1 + L_s \frac{di_1}{dt} + v_1, \tag{2.8}$$

$$e_2 = R_a i_2 + L_s \frac{di_2}{dt} + v_2, \tag{2.9}$$

$$e_3 = R_a i_3 + L_s \frac{di_3}{dt} + v_3, \tag{2.10}$$

where $v_{1,2,3}$ are generator terminal phase voltages (computed using Eqns. (2.16) below), and $i_{1,2,3}$ are the phase currents. The voltage induced in the phase winding by the translator motion is:

$$e_{ph} = K_E \cos\left(\frac{\pi}{\tau} z\right) v(t), \tag{2.11}$$

where z is the displacement of the buoy, $v(t)$ is the vertical velocity of the buoy and the voltage constant K_E is calculated using:

$$K_E = M_s \cdot W_s \cdot N_{\text{ph}} \cdot \phi \cdot v_{\text{av}}, \tag{2.12}$$

where v_{av} is the average buoy speed defined as $v_{av} = \frac{2}{\pi} v_m$ with v_m being the vertical speed amplitude, and $N_{\text{ph}} = N_c \cdot p \cdot q$ is the number of turns per coil for each phase. The induced voltages in the windings for each phase are computed as follows:

$$e_1 = K_E \cos\left(\frac{\pi}{\tau} z\right) v(t), \tag{2.13}$$

$$e_2 = K_E \cos\left(\frac{\pi}{\tau} z - \frac{2\pi}{3}\right) v(t), \tag{2.14}$$

$$e_3 = K_E \cos\left(\frac{\pi}{\tau} z - \frac{4\pi}{3}\right) v(t). \tag{2.15}$$

The generator terminal phase voltages are:

$$v_j = i_j R_L, \qquad j = 1, 2, 3. \tag{2.16}$$

The electromagnetic force for each phase (ph $= 1, 2, 3$) can therefore be computed using:

$$F_{\text{ph}} = N_{\text{ph}} \phi_{\text{ph}} \frac{\pi}{\tau} \sin\left(\frac{\pi z}{\tau}\right) i_{\text{ph}}. \tag{2.17}$$

We will consider two model fidelity levels here. The lower fidelity model, referred to here as the *simple* model, ignores the electromagnetic force in the formulation of the governing differential equations. This means that only the induced current in the circuit is considered without the effect it has on the moving translator. In this model, due to the absence of the electromagnetic force, $v(t)$ will be the same as the wave elevation equation that defines ocean wave elevation as a function of time $u(t)$ (see Eqn. (2.23)). This will be known as the *simple model*, and the corresponding system of governing differential equations is:

$$\frac{d}{dt} i_1 = \frac{e_1 - v_1 - i_1 R_a}{L_s}, \tag{2.18}$$

$$\frac{d}{dt} i_2 = \frac{e_2 - v_2 - i_2 R_a}{L_s}, \tag{2.19}$$

$$\frac{d}{dt} i_3 = \frac{e_3 - v_3 - i_3 R_a}{L_s}, \tag{2.20}$$

where the phase currents (i_1, i_2, i_3). In this model we assume that the buoy (translator) position track the wave elevation exactly (see Section 2.3 for a discussion of the ocean wave model). This is not what occurs in reality, as the difference between wave elevation and buoy position is what provides the buoyancy force that moves the translator to produce electrical energy. This simplification, however, allows investigation of PTO dynamics via a simple third-order dynamic model. A detailed implementation of this model is presented in Appendix A.

The second, higher-fidelity, model accounts for the electromagnetic force and the mechanical dynamics of the buoy. This model is referred to here as the *complex* model. Inclusion of the wave energy converter (WEC) translator dynamics results in a fifth-order dynamic model. Buoy dynamics depend on mass and geometry. Therefore, $v(t)$ will no longer be the same as $u(t)$ since electromagnetic force is not ignored. Instead, it will be defined by the electromagnetic dynamics of the whole system. There are several possible shapes of the buoy, including cylindrical and spherical. Cylindrical buoys are easy to simulate because buoy cross section does not change with respect to vertical position [8, 9]; a cylindrical cross section is used in this model.

The two state variables added to the complex model include the translator position (z) and the translator velocity (v, which is equivalent to buoy velocity). In this model buoy position is decoupled from ocean wave elevation. The

following two equations are added to Eqns. (2.18)-(2.20) to form a set of five differential equations:

$$\frac{d}{dt}z = v, \tag{2.21}$$

$$\frac{d}{dt}v = -\frac{\left[R_r(T) + R_v\right]\left[v - \frac{2\pi}{T}A\cos\left(\frac{2\pi}{T}t\right)\right] + \rho g\pi a^2\left[z - A\sin\left(\frac{2\pi}{T}t\right)\right]}{M + m_r(\infty)}. \tag{2.22}$$

The parameters in Eqns. (2.21) and (2.22) are defined in Section 2.3.

2.3 Wave Model

To understand and quantify the performance of the permanent magnet linear synchronous generator we need a mathematical model of the incoming ocean wave. In both the simple and complex models the incident ocean wave is assumed to be sinusoidal, and in the simple model we assume that the ocean wave elevation is unaffected by the WEC. These are strong assumptions. In reality, ocean waves are irregular. An irregular incident wave field can be modeled as a linear superposition of a finite number of regular, or sinusoidal, wave components [8, 10]. This model is not identical to the real situation, but this simplification allows us to understand how the general model will work. We can understand, through this simplified model, how the PTO will transform the kinetic energy in the incoming ocean wave into electricity.

In the simple model the wave speed amplitude (u_m), which is the maximum vertical speed of the wave, is assumed to be 2.2 m/s, and the period of the wave (T) is assumed to be 12.6 s. With the speed amplitude and period specified, we can now define the wave elevation equation:

$$u(t) = u_m \sin\left(\frac{2\pi t}{T}\right), \tag{2.23}$$

which describes buoy speed as a function of time.

In the complex model, however, the existence of the electromagnetic force complicates the dynamics of the buoy. In the complex model the displacement amplitude of the wave is assumed to be $A = 4$ m. The period T is still assumed to be 12.6 s. While in the simple model we assume that the buoy and translator position is coupled with the wave elevation, the complex model allows for relative motion between the wave and buoy. This allows the generation of net buoyancy force, and requires that we account for the dynamics of the buoy and several other effects. First, we need to consider the volume and mass of the buoy. The mass and displaced volume determine the buoyant force exerted on the buoy by the water. We can calculate the displaced volume based on the buoy radius a and the position of the buoy relative to the wave elevation. The draft b is the depth of the bottom surface of the buoy in still water.

The mass of the buoy is assumed to be $M = 1000$ kg. When the buoy is moving in the water, it will entrain (move) some amount of water with it. This phenomenon gives rise to the term *added mass*, which is the mass of the water

that moves along with the buoy as it oscillates in the water. When formulating a dynamic model of the buoy system the mass used is the sum of the buoy mass and the added mass. According to the calculation in Ref. [8], the added mass $m_r(\infty)$ for the buoy in this report is 289 kg. Since the buoy is moving relative to the water, the radiation resistance R_r, which depends on the geometry of the buoy and the wave frequency [11], will have an effect on the motion of the buoy. R_r is calculated to be 16 Ns/m [8]. In addition, the viscous damping R_v will also play a role in the dynamics, which is calculated to be 717 Ns/m [8]. All the necessary parameters are in Table 2. After taking all these effects into consideration we have the system described as Eq. (2.21) and Eq. (2.22).

Table 2: Heaving Cylinder WEC Parameters for Complex Model [8, 9].

Name	Symbol	Value	Units
Radius	a	0.5	m
Draft	b	1	m
Water depth	h	10	m
Mass	M	1000	kg
Density of water	ρ	1025	kg/m^3
Added mass	$m_r(\infty)$	289	kg
Radiation resistance damping	$R_r(T)$	16	Ns/m
Viscous damping	R_v	717	Ns/m

3 Numerical Studies

3.1 Simulation Results

We simulated the model using MATLAB. We used the solver `ode45`—a variable step Runge-Kutta method—to solve differential equations numerically. The solver `ode45` is appropriate for nonstiff[1] problems when a medium order of accuracy is desired.

Simple Model Results

First we simulated the simpler model, which does not include the electromagnetic force. While the simulation spanned 350 seconds, the time period of primary interest in this study is between 250 s–350 s. After 250 s have elapsed the system has had enough time to reach steady state operating conditions.

As illustrated in Fig. 9 and Fig. 10, z and v both have a sinusoidal shape. The position z is always positive, while the velocity v is symmetric about 0. The maximum and minimum values of z are 8.8235 m and 0, respectively. The velocity v has a maximum of 2.2 m/s and a minimum of -2.2 m/s, as specified

[1] Model stiffness is addressed in Sec. 3.3.

in the previous section. Figure 10 is scaled such that exactly one period of steady-state conditions is displayed.

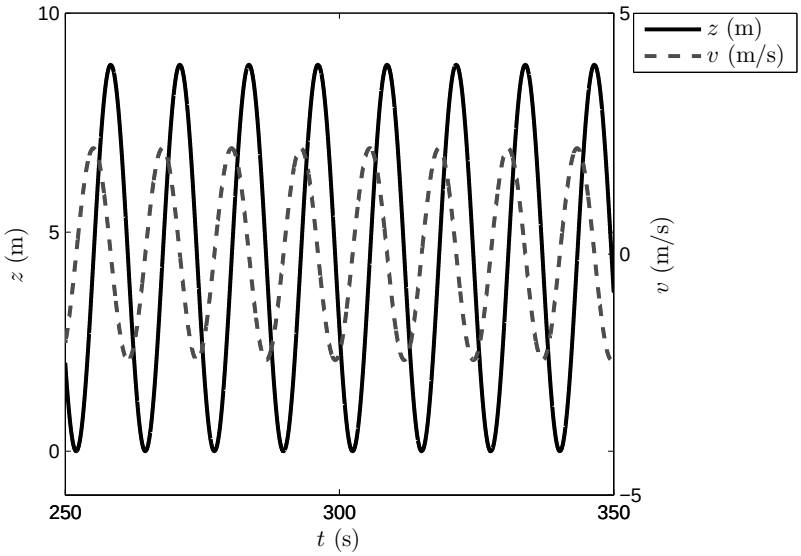

Figure 9: Simple Model Results for Position and Velocity vs. Time.

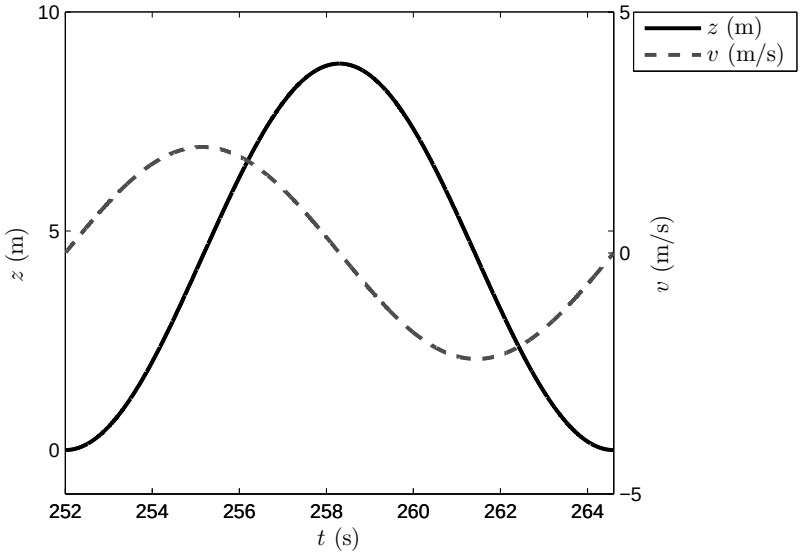

Figure 10: Simple Model Results for Position and Velocity vs. Time—One Period (see Fig. 9).

In Fig. 11 and Fig. 12, which depict current trajectories for all three phases, we can see that there is an rounded envelope shape that bounds the current trajectories. The three currents are symmetric about 0, with a maximum of 253.2 A and a minimum of -253.2 A. Figure 12 is scaled such that exactly one period of steady-state conditions is displayed.

As can be seen from the figures, the electrical dynamics are much faster than the mechanical dynamics (i.e., the position and velocity). The position and the velocity trajectories complete exactly one cycle during one period, whereas the current trajectories complete multiple cycles in one period. The maximum slope of the currents are measured to be approximately 2.42×10^4 A/s, which represents a significant change rate. Also to be noted is that the plot presents a harmonic shape, with the currents being 0 at the beginning, middle and end of each period.

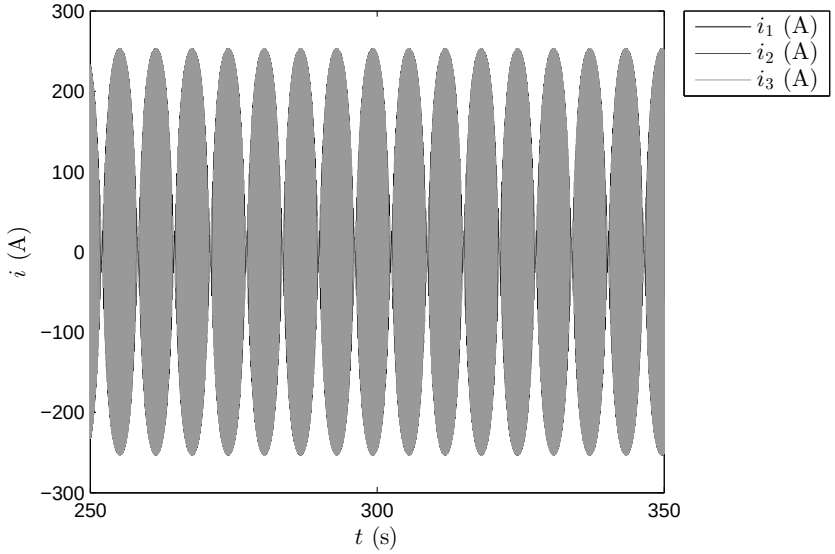

Figure 11: Simple Model Results for Current vs. Time.

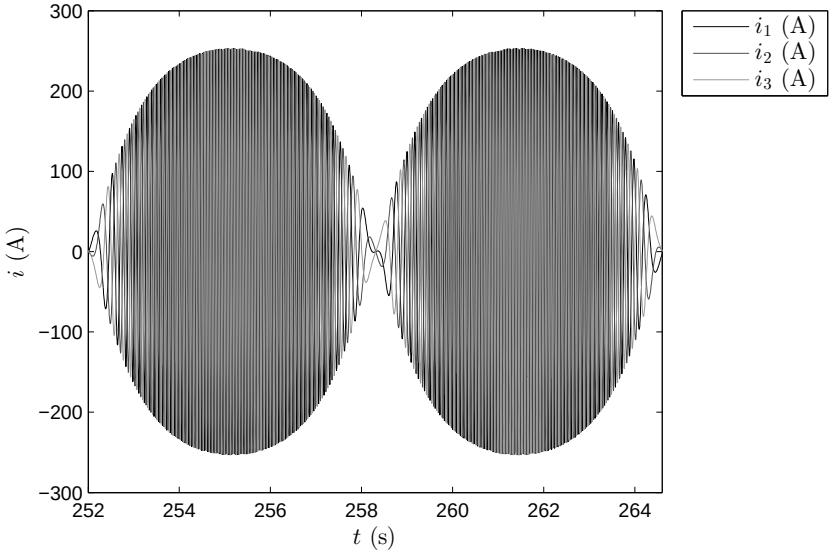

Figure 12: Simple Model Results for Current vs. Time—One Period (see Fig. 11).

Figures 13 and 14 describe the power output of the system, where Fig. 14 is scaled such that exactly one period of steady-state conditions is displayed. Power output ranges from 0 to 6.1332×10^5 W. The power is non-negative since it is calculated using the formula $P = i^2 R_L$. During one period there are two peaks. The average power is 3.7590×10^5 W.

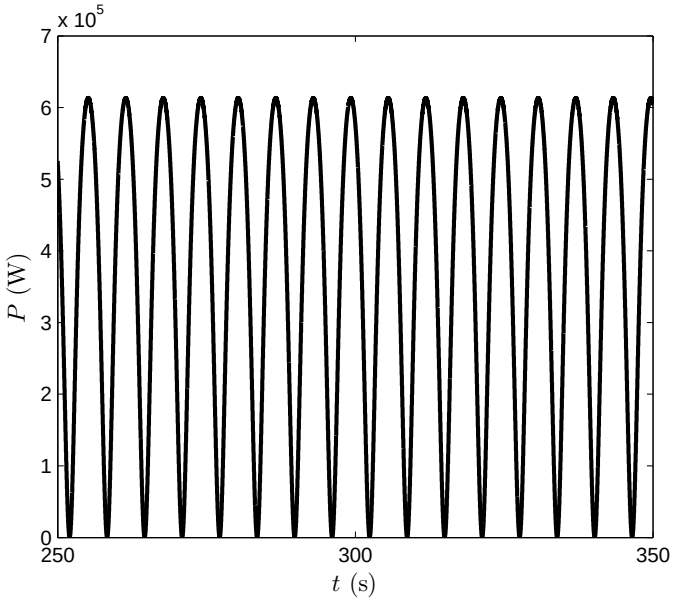

Figure 13: Simple Model Results for Power vs. Time.

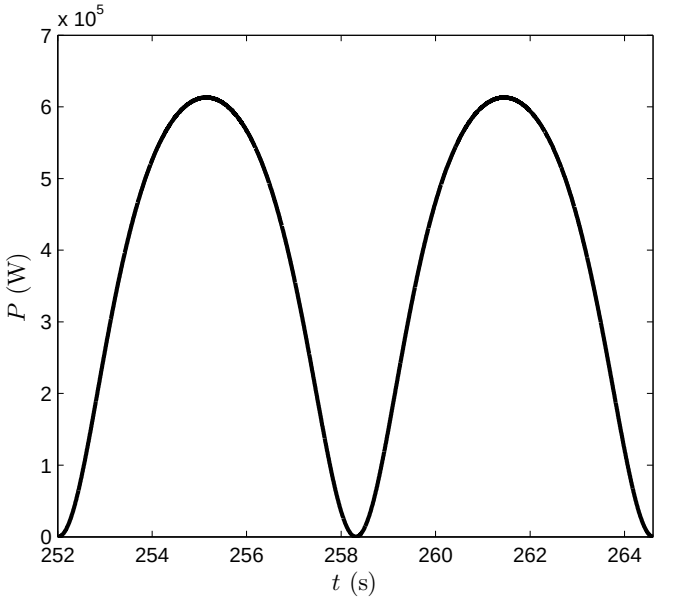

Figure 14: Simple Model Results for Power vs. Time—One Period (see Fig. 13).

Complex Model Results

The complex model was then used in simulating the WEC. As described earlier, this model includes the electromagnetic force as quantified by Eqns. (2.21) and (2.22). The position $z(t)$ and the velocity $v(t)$, depicted in Fig. 15 and Fig. 16, are still periodic. In addition, Fig. 16 shows that v is still close to harmonic, even with the added complexity of the system. The extremes of $v(t)$ are -2.2236 m/s and 3.2256 m/s. In terms of the position, $z(t)$ is still close to harmonic, which is probably due to the damping term in the equations. The position trajectory $z(t)$ has a range of -4.1688m to 4.1688m.

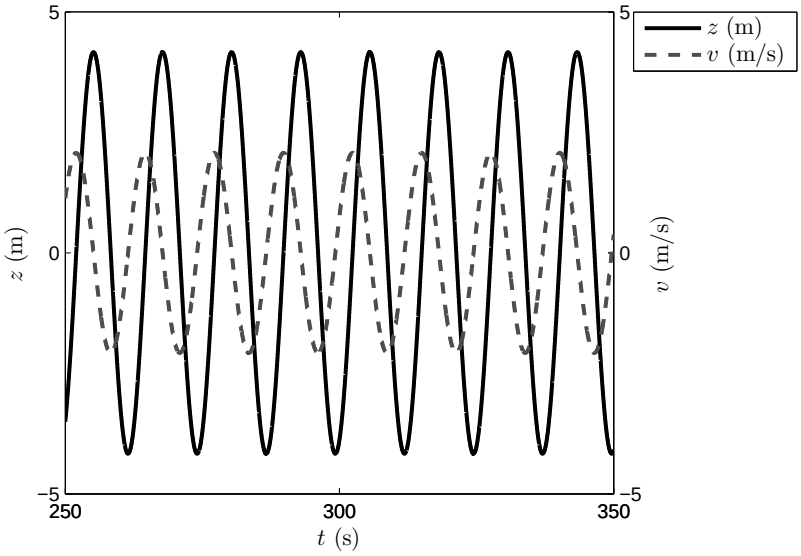

Figure 15: Complex Model Results for Position and Velocity vs. Time.

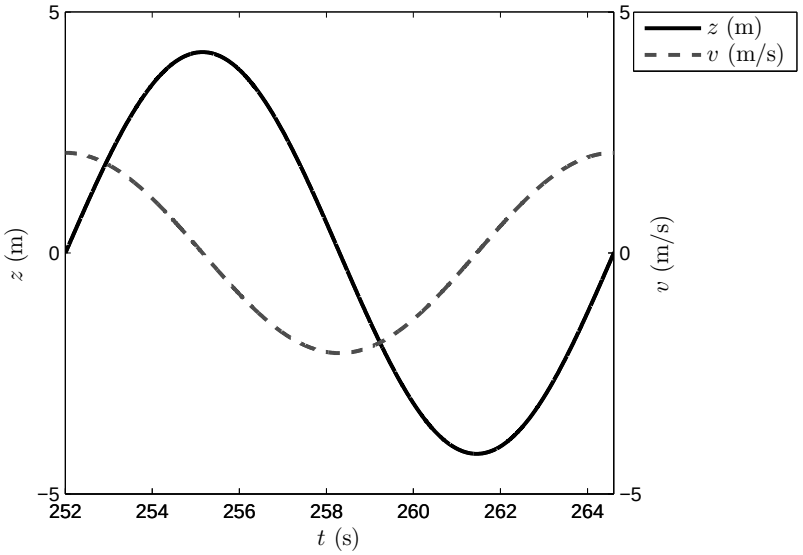

Figure 16: Complex Model Results for Position and Velocity vs. Time—One Period (see Fig. 15).

The current trajectories that resulted from the simulation of the complex model are shown in Figs. 17 and 18. The envelope of the plots in Fig. 17 is similar to the envelope for the simple model simulation results, but not identical because of the different dynamics of the buoy. The envelope still has the rounded shape as before. The range of i is -285 A to 285 A, which is also larger than the previous one. The dynamics are even faster with a maximum slope of 4.00×10^4 A/s. The currents are still symmetric about 0.

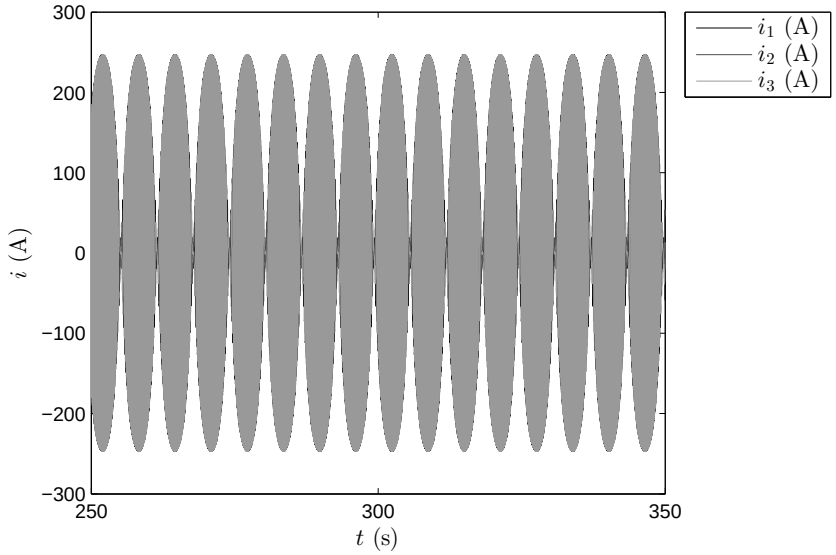

Figure 17: Complex Model Results for Current vs. Time.

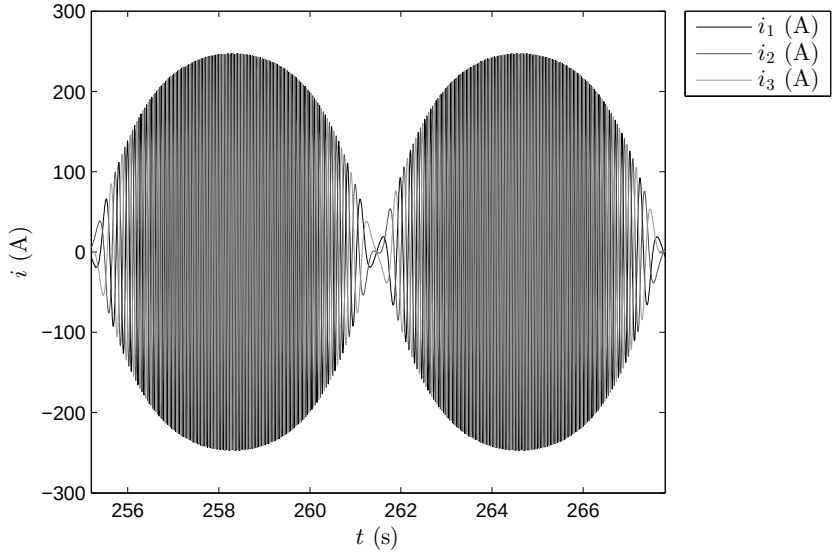

Figure 18: Complex Model Results for Current vs. Time—One Period (see Fig. 17).

The plots of P, namely Fig. 19 and Fig. 20, are also nearly the same as in the simple model simulation. The range, however, is 0 to 7.7994×10^5 W with an average value of 3.5319×10^5 W. While the maximum power output is larger than that of the simple model, the average power is slightly lower than that of the simple model. This indicates that while the power trajectories corresponding to the simple and complex model simulations appear to be the same upon visual inspection, they do in fact have different shapes. In other words, during a certain period of time, the area under the power output curve is smaller, indicating that the shape of the complex model power trajectory is more pointed.

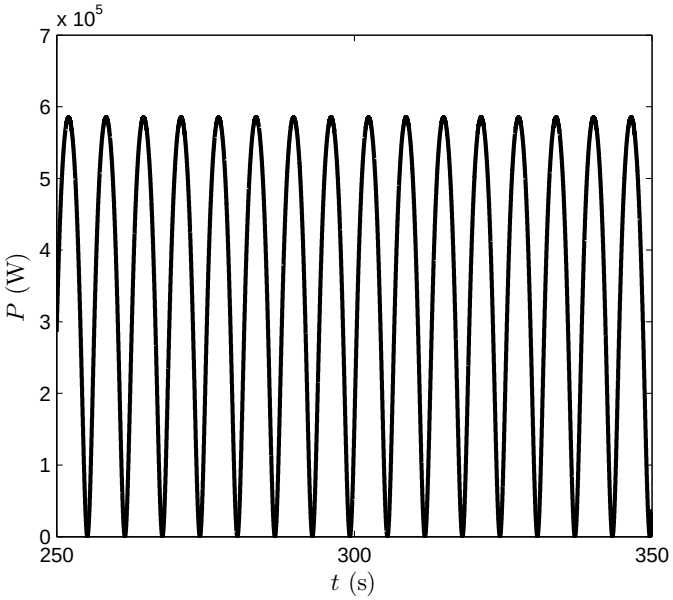

Figure 19: Complex Model Results for Power vs. Time.

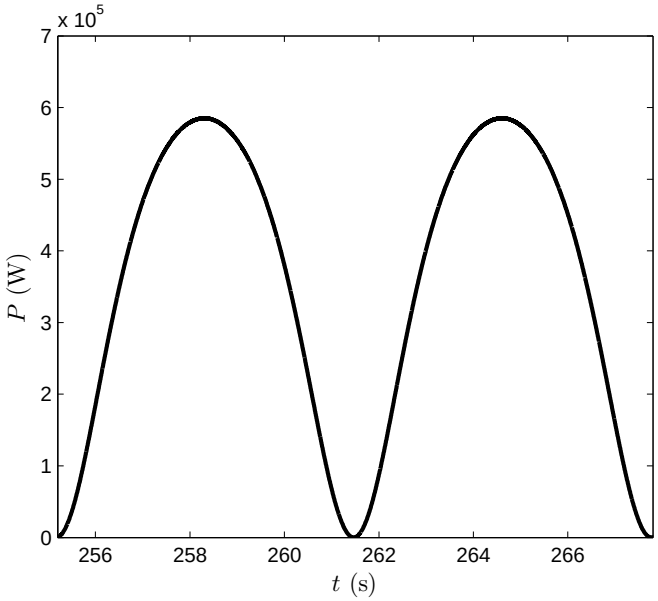

Figure 20: Complex Model Results for Power vs. Time—One Period (see Fig. 19).

3.2 Design Parameter Studies

A parametric study is an activity in which certain parameters are varied through a predetermined range, and the effect of changing these parameters is investigated. In the study presented here one parameter at a time is changed while other parameters are kept unchanged. For each parameter value combination to be tested a simulation is performed to determine the effect of certain parameters on the whole system.

In this report two parameters are studied using the complex model. The first parameter is the slot width b_s, and the second is the air gap g_a.

Slot Width Study

Various values of b_s are studied within the range of 0.022 m to 0.023 m. The maximum power is acquired around $b_s = 0.02248$ m. Figure 21 illustrates energy extraction over one steady-state period as a function of b_s. It is depicted using a semi log plot as the energy values span several orders of magnitude. This plot exhibits a large peak with a maximum energy extraction value of 9.0396×10^{13} J.

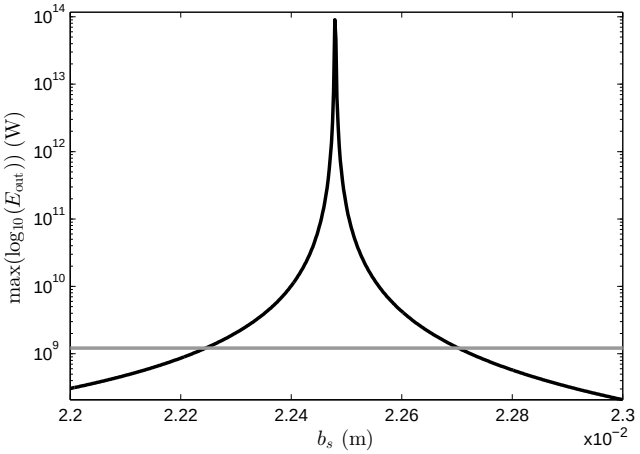

Figure 21: Slot Width (b_s) Parameter Study (The horizontal line represents the maximum energy that can be extracted from the incoming ocean wave).

Figure 22 illustrates the power trajectory for the system design that corresponds to the maximum energy design in the slot width parametric study (i.e., $b_s = 0.02248$ m).

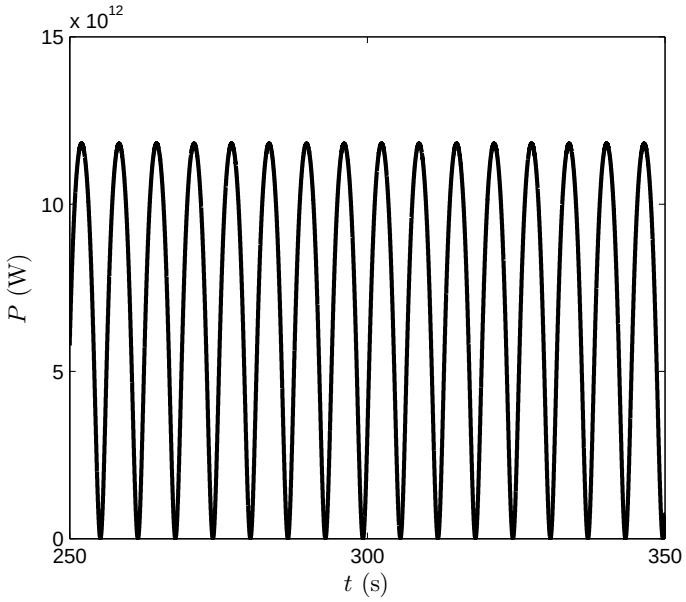

Figure 22: Power Trajectory for Slot Width Value Maximizing Peak Power of the Complex Model ($b_s = 0.0225$ m).

The peak in the middle suggests resonant behavior. Given the magnitude of energy extraction at the peak, the validity of the model should be questioned. For example, for a given buoy size and wave conditions, it is possible to calculate the maximum amount of energy that can be extracted from an ocean wave. If all of the energy is extracted, the wave will be completely destroyed [11]. A practical wave energy converter will only be able to extract a fraction of the total available energy. Using the approach described by Herber and Allison [8], the maximum available energy in the wave was calculated and plotted as a horizontal line in Fig. 21.

Clearly values of b_s that produce energy values above this line in the simulation will not produce these energy values in a physical system. This model is not capturing some element of the real system behavior. Simply setting $b_s = 0.02248$ m cannot be expected to produce optimal system behavior. In addition to improving model fidelity, system optimization would require the simultaneous consideration of all important design variables, not just a simple study of one parameter at a time[2].

Figures 23 and 24 illustrate the current trajectories for the design where b_s is 0.0225 m. It can be observed that the current trajectories are very dynamic with larger ranges, meaning that more energy can be produced by this system design.

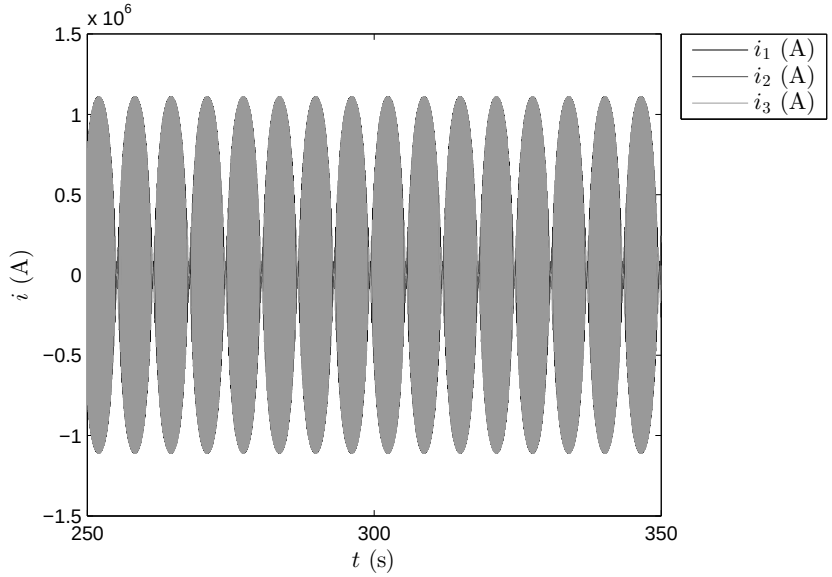

Figure 23: Current vs. Time for Slot Width Value Maximizing Peak Power of the Complex Model ($b_s = 0.0225$ m).

[2]While such an optimization effort is beyond the scope of this report, it is the subject of ongoing research at the UIUC Engineering System Design Laboratory.

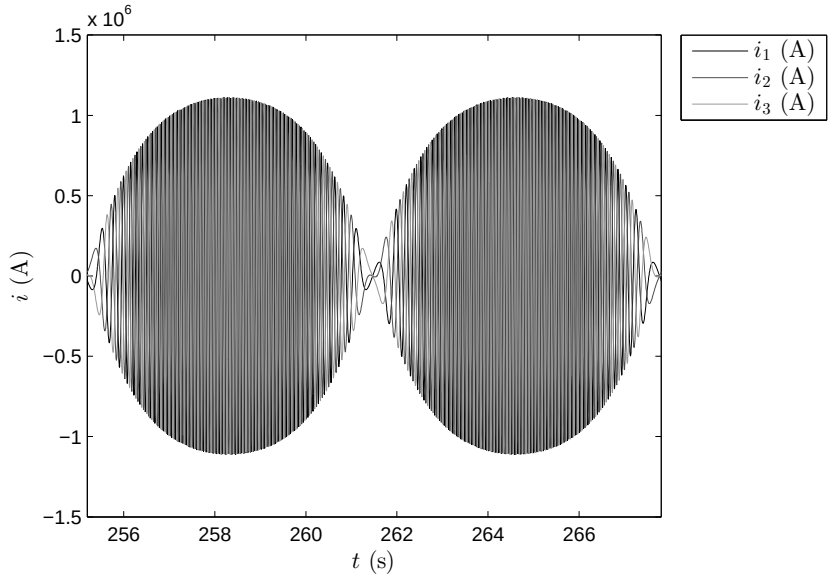

Figure 24: Current vs. Time for Slot Width Value Maximizing Peak Power of the Complex Model—One Period (see Fig. 23).

To summarize, according to the simulation results, the optimal slot width b_s is 0.0225 m. This will give a peak power of 1.5741×10^{13} W, according to Fig. 22. That produces 9.0396×10^{13} J per period. However, other constraints may prevent b_s from achieving the optimal value. The model here likely is not complete, and design variable interactions should be considered as well[3].

Air Gap Study

The second parameter studied here is the air gap g_a. Various values of g_a are studied within the range of 0.0035 m and 0.0045 m, and the maximum power is realized at $g_a = 0.004$ m. The maximum energy extracted during a period is 2.4494×10^{13} J. The energy extraction per period as a function of g_a is illustrated in Fig. 25, and the power trajectory that corresponds to the maximum energy extraction is shown in Fig. 27.

[3]Determining the underlying cause of this model inaccuracy is beyond the scope of this report, and is a topic for future research.

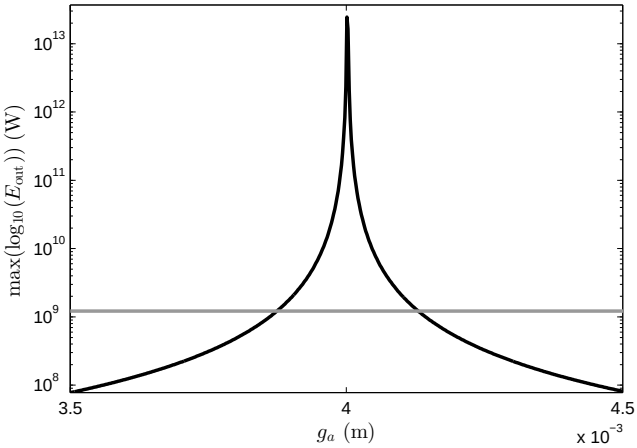

Figure 25: Air Gap (g_a) Parameter Study (The horizontal line represents the maximum energy that can be extracted from the incoming ocean wave).

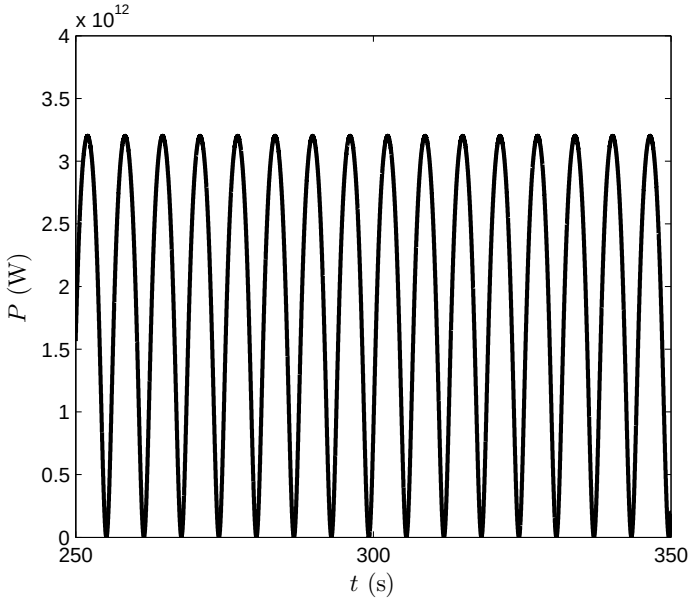

Figure 26: m

Figure 27: Power Trajectory for Air Gap Value Maximizing Peak Power of the Complex Model ($g_a = 0.0040$ m).

As can be seen from Fig. 25, the range of g_a values that produce large energy

values is also very small. The peak in the middle also suggests that there is resonance occurring in the system when certain values of g_a are chosen. Again, the horizontal line represents the maximum amount of energy that can be possibly extracted from the incoming ocean wave, calculated according to Ref. [8]. This means that we actually can't reach the peak energy extraction value shown in this figure.

The current trajectories that correspond to the design that maximizes energy extraction (i.e., g_a is 0.004 m) are illustrated in Figs. 28 and 29. The behavior here is very similar to what was observed in the slot width study. Ranges of resonance exist in both parametric studies, and the current trajectories that correspond to the peak energy extraction design have very large amplitudes. According to the model used here, $g_a = 0.004$ m produces a maximum peak power of 4.2683×10^{12} W, and produces 2.4494×10^{13} J per period in steady state. As noted before, other constraints will prevent realization of the predicted maximum energy extraction.

Only two parameters of the generator are studied here. Other parameters, especially other independent physical variables, are a subject for further study.

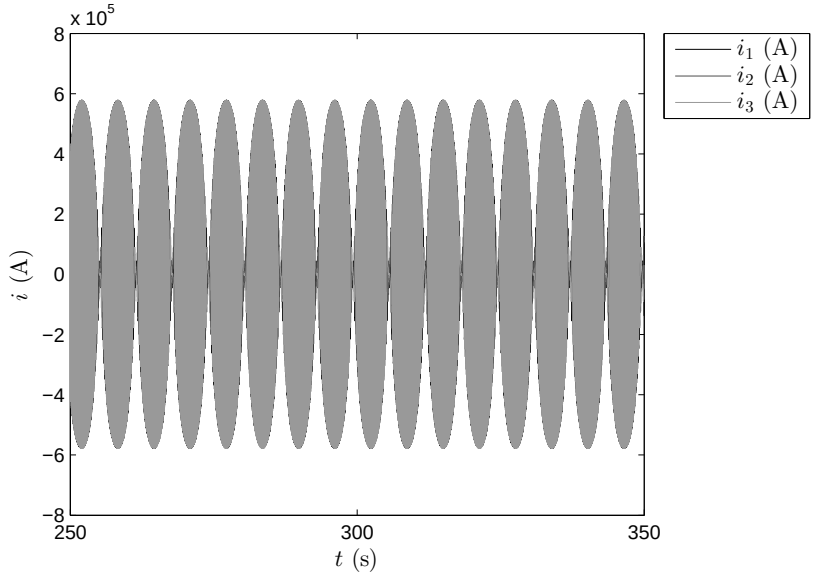

Figure 28: Current vs. Time for Air Gap Value Maximizing Peak Power of the Complex Model ($g_a = 0.0040$ m).

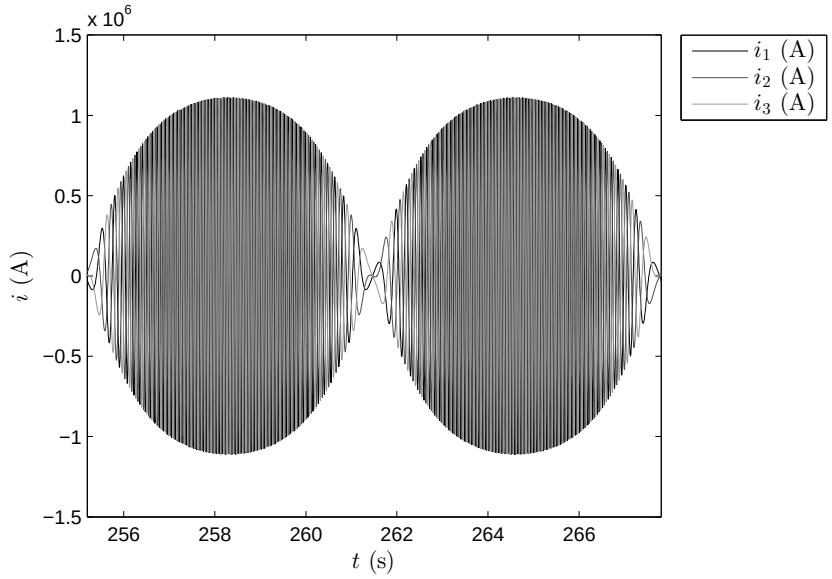

Figure 29: Current vs. Time for Air Gap Value Maximizing Peak Power of the Complex Model—One Period (see Fig. 28).

3.3 Model Stiffness Study

The stiffness of the system modeled in this report was also studied. A dynamic model is often thought of as stiff if it involves both fast and slow dynamics. Here the mechanical dynamics are much slower than the electrical dynamics. Another definition of model stiffness is that stiff systems may be simulated more efficiently using an implicit solver for ordinary differential equations (i.e., a stiff solver).

One way of determining stiffness is to evaluate the time steps required to simulate a system using both a stiff and non-stiff solver. Here `ode45` was the non-stiff solver used, and `ode15s` was the stiff solver used. Figure 30 illustrates how the time step sizes change through time for `ode45` based on the simple model, and Fig. 31 illustrates time step sizes for `ode15s` based on the simple model.

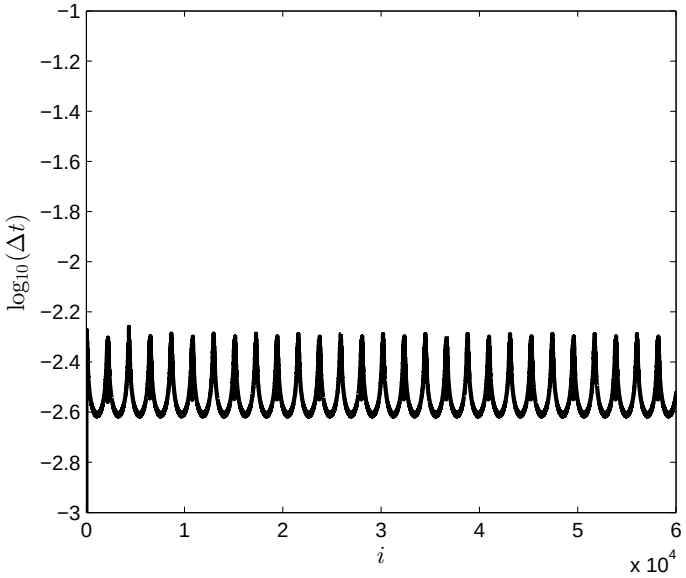

Figure 30: Plot of Time-Steps using the Simple Model with `ode45`.

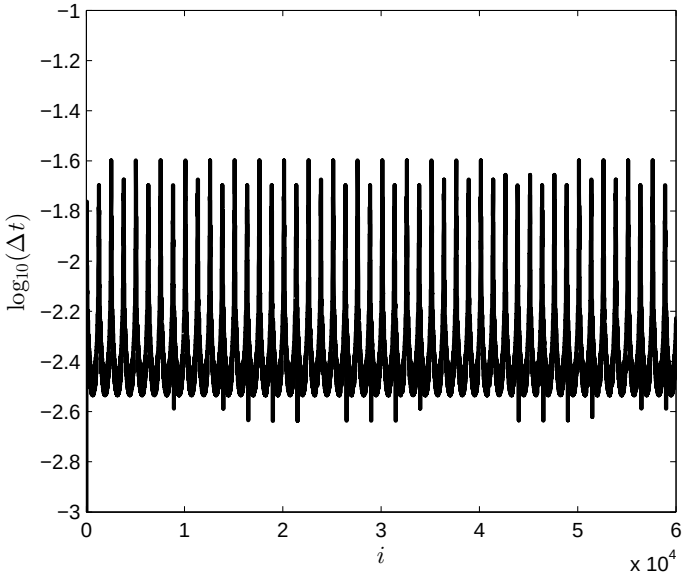

Figure 31: Plot of Time-Steps using the Simple Model with `ode15s`.

It is clear from Fig. 30 that the time steps remain very small (they differ by

less than an order of magnitude). This means that `ode45`, a non-stiff solver, but use very small time steps throughout the entire simulation to maintain the required accuracy. In other words, it struggles to solve the system of differential equations efficiently. Figure 31, on the other hand, shows that `ode15s` is able to use much larger time steps periodically and still maintain accuracy. After being driven to a small step size to maintain accuracy due to rapid change in state, the stiff solver is able to 'recover' to a larger step size, whereas the non-stiff solver is unable to maintain accuracy unless step sizes are kept very small. In other words, the stiff solver solves the system more efficiently than the non-stiff solver, so this is evidence that this system model exhibits stiffness. This is common in models of physical systems, and it is important to address the potential for dynamic stiffness when developing models for the design of physical systems.

A similar result was observed when comparing the `ode45` and `ode15s` solutions based on the complex model. These results are illustrated in Figs. 32 and 33. The range of step size values with the complex model is a bit larger than with the simple model, indicating somewhat increased system stiffness. In addition, the complex model takes some time to achieve steady-state time step behavior.

The total number of time steps for each simulation was also recorded. Table 3 summarizes these results. An additional non-stiff solver (`ode23`) was tested as well. Based on the number of required time steps, `ode23` performs similarly to `ode45`. For both the simple and complex models, the total number of required time steps (which is related to computational expense) is reduced significantly when switching to a stiff solver. This is additional evidence that the system model exhibits stiff behavior.

Table 3: Number of Time-Steps for Various ODE Solvers.

	`ode45`	`ode23`	`ode15s`
Simple	119708	116235	69655
Complex	117676	110316	66583

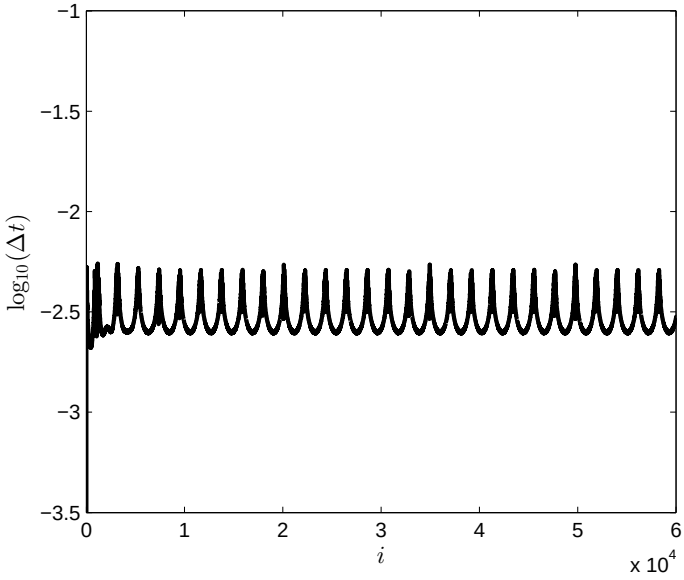

Figure 32: Plot of Time-Steps using the Complex Model with `ode45`.

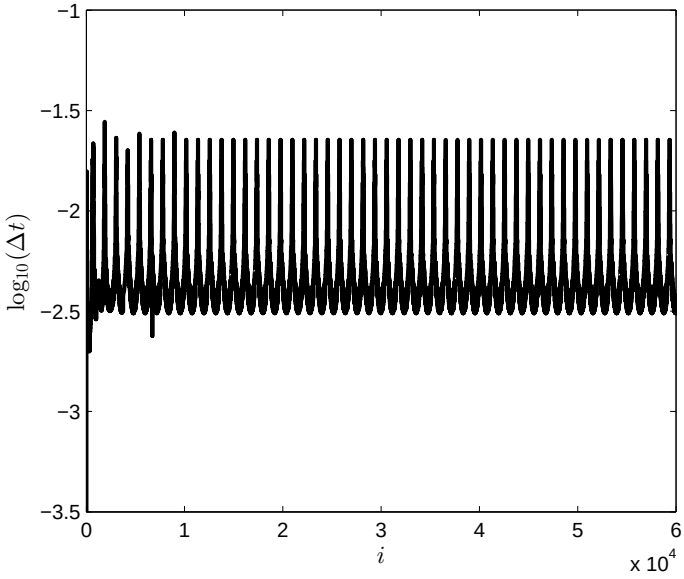

Figure 33: Plot of Time-Steps using the Complex Model with `ode15s`.

4 Conclusion

Wave energy extraction is of great potential importance given that fossil fuel as an energy source is limited and non-renewable. The design of a permanent magnet linear synchronous generator for wave energy extraction can greatly improve the efficiency. In this report the necessary physics theories for modeling and designing a permanent magnet linear synchronous generator are reviewed. Then a model of a permanent magnet linear synchronous generator is constructed, involving both independent and dependent parameters. It is simulated in MATLAB® for specific parameters. Two of the independent physical parameters of the generator were studied further using parametric sweeps. The results indicate that there is potential for improvements of the specific permanent magnet linear synchronous generator modeled in this work, as well as potential for improving the system model. Future work may focus on deeper study of the independent parameters of the model, interactions between independent parameters, improved-fidelity modeling (including more detailed models of other system components), and design optimization studies.

Acknowledgments

This report is based on the prior work of James T. Allison, Allen Kaitharath and Daniel R. Herber [8, 9]. The work presented in this report was conducted under Prof. Allison's supervision and with the guidance of Daniel R. Herber. Significant edits and feedback have been provided by both Prof. Allison and Daniel R. Herber.

References

[1] N. M. Kimoulakis, A. G. Kladas, and J. A. Tegopoulos. "Power Generation Optimization from Sea Waves by Using a Permanent Magnet Linear Generator Drive". In: *IEEE Transactions on Magnetics* 44.6 (2008), pp. 1530–1533. DOI: 10.1109/TMAG.2007.914854.

[2] R. Parthasarathy. "Linear PM Generator for Wave Energy Conversion". Master's Thesis. Anna University, 2012. URL: http://etd.lsu.edu/docs/available/etd-04182012-121521/unrestricted/parthasarathythesis.pdf.

[3] S. A. Nasar and I. Boldea. *Linear Electric Motors: Theory, Design and Practical Applications*. Prentice Hall, 1987. ISBN: 9780135368633.

[4] O. Danielsson. "Design of a Linear Generator for Wave Energy Plant". Master's Thesis. Uppsala University, 2003. URL: http://www.el.angstrom.uu.se/meny/artiklar/design%20of%20a%20linear%20generator%20for%20wave%20energy%20plant4.pdf.

[5] A. W. van Zyl et al. "Comparison of Force to Weight Ratios Between a Single-Sided Linear Synchronous Motor and a Tubular Linear Synchronous Motor". In: *IEEE International Electric Machines and Drives Conference 1999*. Seattle, WA, USA, 1999, pp. 571–573. ISBN: 0780352939. DOI: 10.1109/IEMDC.1999.769178.

[6] F. W. Carter. "Note on Air-Gap and Interpolar Induction". In: *Journal of the Institution of Electrical Engineers* 29 (1900), pp. 925–933. DOI: 10.1049/jiee-1.1900.0095.

[7] F. W. Carter. "Air-Gap Induction". In: *Electric World and Engineer* 38.22 (1901), pp. 884–888. URL: http://hdl.handle.net/2027/uva.x030741299.

[8] J. T. Allison and D. R. Herber. "Wave Energy Extraction Maximization in Irregular Ocean Waves Using Pseudospectral Methods". In: *ASME 2013 International Design Engineering Technical Conferences and Computers and Information in Engineering Conference*. Portland, OR, USA, 2013. URL: http://systemdesign.illinois.edu/publications/Her13a.pdf.

[9] J. T. Allison, A. Kaitharath, and D. R. Herber. "Wave Energy Extraction Maximization Using Direct Transcription". In: *ASME 2012 International Mechanical Engineering Congress and Exposition*. Houston, TX, USA, 2012. URL: `http://systemdesign.illinois.edu/publications/All12c.pdf`.

[10] T. Jeans et al. "Irregular Deep Ocean Wave Energy Conversion Using a Cycloidal Wave Energy Converter". In: *9th European Wave and Tidal Energy Conference*. Southampton, UK, 2011.

[11] J. Falnes. "Wave-Energy Absorption by Oscillating Bodies". In: *Cambridge University Press* (2002).

A Appendix: Modeling Code

Simulation.m

```
% This script accepts the values for the independent variables ...
    bs and ga
% and also a flag indicating which model should be used. x(1) is the
% position of the buoy. x(2) is the velocity of the buoy. x(3), ...
    x(4) and
% x(5) are the three currents. The outputs are t, x and Pout, ...
    which is the
% output power.
function [t,x,Pout] = Simulation(bs,ga,flag)

    % run simulation
    [t,x] = ode45(@(t,x) LPM_3Phase(t,x,bs,ga,flag), [0 350], [0 ...
        0 0 0 0]);

    % calculate power
    RL = 7.5; %Ohm
    v(:,1) = x(:,3)*RL;
    v(:,2) = x(:,4)*RL;
    v(:,3) = x(:,5)*RL;
    Pin = x(:,3).*v(:,1) + x(:,4).*v(:,2) + x(:,5).*v(:,3);
    Pout = Pin.*0.85;

end

function dx = LPM_3Phase(t,x,bs,ga,flag)
    dx = zeros(5,1);
    p = 6;
    q = 1;
    m = 3;
    N = zeros(1,3);
    for i = 1:3
        N(i) = 82*p*q;
    end
    L = 0.432; %m
    taup = L/p; %m
    taut = taup./(m*q); %m
    % bs = 0.016; %m
    bt = taut - bs; %m
    % ga = 0.002; %m
    Kc = taut*(5*ga+bs)/(taut*(5*ga+bs)-bs^2);
    geq = Kc*ga;
    hm = 0.006; %m
    Br = 1.2; %T
    mu0 = 4*pi*10^(-7);
    Hc = 905000;
    phi = zeros(1,3);
    for i = 1:3
        phi(i) = (Br*hm*Hc*mu0)/(hm*Hc*mu0 - geq*Br);
    end

    if flag == 1 % Simple
        um = 2.2; %m/s
```

```
49          uav = 2/pi*um; %m/s
50          T = 12.6; %s
51          Ra = 1.5; %Ohm
52          Ls = 0.115; %H
53          RL = 7.5; %Ohm
54          Ms = 4; %number of armatures
55          Ws = 0.2; %m
56          KE = Ms*Ws*N(i)*phi(i)*uav;
57          % u = um*sin(omegam*t);
58          u = um.*sin(2*pi.*t./T);
59          du = 2*pi.*um./T*cos(2*pi.*t./T);
60          e = zeros(1,3);
61          e(1) = KE*cos(pi.*x(1)./taup)*u;
62          e(2) = KE*cos(pi.*x(1)./taup - 2*pi/3)*u;
63          e(3) = KE*cos(pi.*x(1)./taup - 4*pi/3)*u;
64          v = zeros(1,3);
65          v(1) = x(3)*RL;
66          v(2) = x(4)*RL;
67          v(3) = x(5)*RL;
68          F = zeros(1,3);
69          for i = 1:3
70              F(i) = ...
                    N(i).*phi(i).*pi./taup.*sin(pi.*x(1)./taup).*x(i ...
                    + 2);
71          end
72          dx(1) = u; % u
73          dx(2) = du;
74      elseif flag == 2 % Complex
75          um = 2.2; %m/s
76          uav = 2/pi*um; %m/s
77          T = 12.6; %s
78          A = 4; %um*T/(2*pi); %m
79          Ra = 1.5; %Ohm
80          Ls = 0.115; %H
81          RL = 7.5; %Ohm
82          Ms = 4; %number of armatures
83          Ws = 0.2; %m
84          KE = Ms*Ws*N(i)*phi(i)*uav;
85          % u = um*sin(omegam*t);
86          u = x(2);
87          e = zeros(1,3);
88          e(1) = KE*cos(pi.*x(1)./taup).*u;
89          e(2) = KE*cos(pi.*x(1)./taup - 2*pi/3).*u;
90          e(3) = KE*cos(pi.*x(1)./taup - 4*pi/3).*u;
91          v = zeros(1,3);
92          v(1) = x(3)*RL;
93          v(2) = x(4)*RL;
94          v(3) = x(5)*RL;
95          F = zeros(1,3);
96          for i = 1:3
97              F(i) = ...
                    N(i).*phi(i).*pi./taup.*sin(pi.*x(1)./taup).*x(i ...
                    + 2);
98          end
99          rho = 1025; %kg/m^3
100         g = 9.81; %m/s^2
101         a = 0.5; %m
```

```
102          b = 1; %m
103          h = 10; %m
104          M = 1000; %kg
105          mr = 289; %kg
106          Rr = 16; %Ns/m
107          Rv = 717; %Ns/m
108          dx(1) = x(2);
109          dx(2) = -((Rr + Rv).*(x(2) - ...
                 2.*pi.*A./T.*cos(2.*pi.*t./T)) +...
110              rho.*g.*pi.*a.^2.*(x(1) - A.*sin(2.*pi.*t./T))./(M ...
                     + mr);
111      end
112      dx(3) = (e(1) - v(1) - x(3)*Ra)/Ls;
113      dx(4) = (e(2) - v(2) - x(4)*Ra)/Ls;
114      dx(5) = (e(3) - v(3) - x(5)*Ra)/Ls;
115  end
```

Parameter _ Studies.m

```
1  % This script will run the simulation for 500 different values ...
       within the
2  % range given for two independent variables, bs and ga. The ...
       results, which
3  % is the power output, will be analyzed and plotted.
4  path = msavename(mfilename('fullpath'),'Saved_Data');
5  fig_index = 0;
6
7  %% bs study
8  start = 0.022;
9  finish = 0.023;
10 N = 500;
11 array = linspace(start,finish,N);
12
13 results = zeros(N,1);
14 parfor i = 1:N
15
16     bs = array(i); % m
17     ga = 0.002; % m
18     [t,x,Pout] = Simulation(bs,ga,2);
19
20     t1 = find(t <= 250);
21     i1 = find(t1 == t1(end));
22     T = 12.6; %s
23     n = (t(end) - t(i1))./T;
24     periodT = t(i1:end);
25     periodP = Pout(i1:end);
26     E = trapz(periodT, periodP)./n;
27     results(i) = E; % max(Pout);
28
29 end
30 save(strcat(path, 'bs-study'))
31
32 %% figure // bs-study
33 %load(strcat(path, 'bs-study'))
34 data.fig_name = 'bs-study';
35 % label names
```

```
36 data.xname = '$b_s$ (m)';
37 data.yname = '$\max(P_{\mathrm{out}})$ (W)';
38 % state data
39 data.x1 = array;
40 data.y1 = results;   % position
41 % axis limits
42 data.xmin = start;
43 data.xmax = finish;
44 data.ymin = min(results);
45 data.ymax = max(results);
46
47 fig_index = fig_index + 1;
48 create_figure(data,fig_index,1)
49 save2pdf(strcat(path,data.fig_name,'.pdf'),fig_index,600)
50
51 %% figure // Power-Complex-bs
52 % Simulate using optimal bs
53 bs_index = find(results == max(results));
54 bs = bs_index; % m
55 ga = 0.002; % m
56 [t,x,Pout] = Simulation(bs,ga,2);
57
58 data.fig_name = 'Power-Complex-bs';
59 % label names
60 data.xname = '$t$ (s)';
61 data.yname = '$P$ (W)';
62 % state data
63 data.x1 = t;
64 data.y1 = Pout;   % power
65 % axis limits
66 data.xmin = 250;
67 data.xmax = 350;
68 data.ymin = 0;
69 data.ymax = 1.5*10^13;
70
71 fig_index = fig_index + 1;
72 create_figure(data,fig_index,1)
73 save2pdf(strcat(path,data.fig_name,'.pdf'),fig_index,600)
74
75 %% figure // Buoy-Complex-bs
76 % Simulate using optimal bs
77 bs_index = find(results == max(results));
78 bs = bs_index; % m
79 ga = 0.002; % m
80 [t,x,Pout] = Simulation(bs,ga,2);
81
82 data.fig_name = 'Buoy-Complex-bs';
83 % label names
84 data.xname = '$t$ (s)';
85 data.y1name = '$z$ (m)';
86 data.y2name = '$v$ (m/s)';
87 % state data
88 data.x1 = t;
89 data.x2 = t;
90 data.y1 = x(:,1);   % position
91 data.y2 = x(:,2);   % speed
92 % axis limits
```

```
93  data.xmin = 250;
94  data.xmax = 350;
95  data.y1min = -5;
96  data.y1max = 5;
97  data.y2min = -5;
98  data.y2max = 5;
99
100 fig_index = fig_index + 1;
101 create_figure(data,fig_index,2)
102 save2pdf(strcat(path,data.fig_name,'.pdf'),fig_index,600)
103
104 %% figure // Buoy-Complex-Zoom-bs
105 % Simulate using optimal bs
106 bs_index = find(results == max(results));
107 bs = bs_index; % m
108 ga = 0.002; % m
109 [t,x,Pout] = Simulation(bs,ga,2);
110
111 data.fig_name = 'Buoy-Complex-Zoom-bs';
112 % label names
113 data.xname = '$t$ (s)';
114 data.y1name = '$z$ (m)';
115 data.y2name = '$v$ (m/s)';
116 % state data
117 data.x1 = t;
118 data.x2 = t;
119 data.y1 = x(:,1);   % position
120 data.y2 = x(:,2);   % speed
121 % axis limits
122 data.xmin = 252;
123 data.xmax = 264.6;
124 data.y1min = -5;
125 data.y1max = 5;
126 data.y2min = -5;
127 data.y2max = 5;
128
129 fig_index = fig_index + 1;
130 create_figure(data,fig_index,2)
131 save2pdf(strcat(path,data.fig_name,'.pdf'),fig_index,600)
132
133 %% figure // Current-Complex-bs
134 % Simulate using optimal bs
135 bs_index = find(results == max(results));
136 bs = bs_index; % m
137 ga = 0.002; % m
138 [t,x,Pout] = Simulation(bs,ga,2);
139
140 data.fig_name = 'Current-Complex-bs';
141 % label names
142 data.xname = '$t$ (s)';
143 data.yname = '$i$ (A)';
144 data.y1name = '$i_1$ (A)';
145 data.y2name = '$i_2$ (A)';
146 data.y3name = '$i_3$ (A)';
147 % state data
148 data.x1 = t;
149 data.y1 = x(:,3);   % current 1
```

```
data.y2 = x(:,4);   % current 2
data.y3 = x(:,5);   % current 3
% axis limits
data.xmin = 250;
data.xmax = 350;
data.ymin = -1.5*10^6;
data.ymax = 1.5*10^6;

fig_index = fig_index + 1;
create_figure(data,fig_index,3)
save2pdf(strcat(path,data.fig_name,'.pdf'),fig_index,600)

%% figure // Current-Complex-Zoom-bs
% Simulate using optimal bs
bs_index = find(results == max(results));
bs = bs_index; % m
ga = 0.002; % m
[t,x,Pout] = Simulation_Complex(bs,ga,2);

data.fig_name = 'Current-Complex-Zoom-bs';
% label names
data.xname = '$t$ (s)';
data.yname = '$i$ (A)';
data.y1name = '$i_1$ (A)';
data.y2name = '$i_2$ (A)';
data.y3name = '$i_3$ (A)';
% state data
data.x1 = t;
data.y1 = x(:,3);   % current 1
data.y2 = x(:,4);   % current 2
data.y3 = x(:,5);   % current 3
% axis limits
data.xmin = 255.2;
data.xmax = 267.8;
data.ymin = -1.5*10^6;
data.ymax = 1.5*10^6;

fig_index = fig_index + 1;
create_figure(data,fig_index,3)
save2pdf(strcat(path,data.fig_name,'.pdf'),fig_index,600)

%% ga study
start = 0.0035;
finish = 0.0045;
N = 500;
array = linspace(start,finish,N);

results = zeros(N,1);
parfor i = 1:N

    bs = 0.016; % m
    ga = array(i); % m
    [t,x,Pout] = Simulation(bs,ga,2);

    t1 = find(t <= 250);
    i1 = find(t1 == t1(end));
    T = 12.6; %s
```

```
207      n = (t(end) - t(i1))./T;
208      periodT = t(i1:end);
209      periodP = Pout(i1:end);
210      E = trapz(periodT, periodP)./n;
211      results(i) = E; % max(Pout);
212
213  end
214  save(strcat(path, 'ga_study'))
215
216  %% figure // ga_study
217  %load(strcat(path, 'bs_study'))
218  data.fig_name = 'ga_study';
219  % label names
220  data.xname = '$g_a$ (m)';
221  data.yname = '$\max(P_{\mathrm{out}})$ (W)';
222  % state data
223  data.x1 = array;
224  data.y1 = results;   % position
225  % axis limits
226  data.xmin = start;
227  data.xmax = finish;
228  data.ymin = min(results);
229  data.ymax = 8.6*10^12;
230
231  fig_index = fig_index + 1;
232  create_figure(data,fig_index,1)
233  save2pdf(strcat(path,data.fig_name,'.pdf'),fig_index,600)
234
235  %% figure // Power_Complex_ga
236  % Simulate using optimal ga
237  ga_index = find(results == max(results));
238  bs = 0.016; % m
239  ga = ga_index; % m
240  [t,x,Pout] = Simulation(bs,ga,2);
241
242  data.fig_name = 'Power_Complex_ga';
243  % label names
244  data.xname = '$t$ (s)';
245  data.yname = '$P$ (W)';
246  % state data
247  data.x1 = t;
248  data.y1 = Pout;   % power
249  % axis limits
250  data.xmin = 250;
251  data.xmax = 350;
252  data.ymin = 0;
253  data.ymax = 4*10^12;
254
255  fig_index = fig_index + 1;
256  create_figure(data,fig_index,1)
257  save2pdf(strcat(path,data.fig_name,'.pdf'),fig_index,600)
258
259  %% figure // Buoy_Complex_ga
260  % Simulate using optimal ga
261  ga_index = find(results == max(results));
262  bs = 0.016; % m
263  ga = ga_index; % m
```

```
[t,x,Pout] = Simulation(bs,ga,2);

data.fig_name = 'Buoy-Complex-ga';
% label names
data.xname = '$t$ (s)';
data.y1name = '$z$ (m)';
data.y2name = '$v$ (m/s)';
% state data
data.x1 = t;
data.x2 = t;
data.y1 = x(:,1);   % position
data.y2 = x(:,2);   % speed
% axis limits
data.xmin = 250;
data.xmax = 350;
data.y1min = -5;
data.y1max = 5;
data.y2min = -5;
data.y2max = 5;

fig_index = fig_index + 1;
create_figure(data,fig_index,2)
save2pdf(strcat(path,data.fig_name,'.pdf'),fig_index,600)

%% figure // Buoy-Complex-Zoom-ga
% Simulate using optimal ga
ga_index = find(results == max(results));
bs = 0.016; % m
ga = ga_index; % m
[t,x,Pout] = Simulation(bs,ga,2);

data.fig_name = 'Buoy-Complex-Zoom-ga';
% label names
data.xname = '$t$ (s)';
data.y1name = '$z$ (m)';
data.y2name = '$v$ (m/s)';
% state data
data.x1 = t;
data.x2 = t;
data.y1 = x(:,1);   % position
data.y2 = x(:,2);   % speed
% axis limits
data.xmin = 252;
data.xmax = 264.6;
data.y1min = -5;
data.y1max = 5;
data.y2min = -5;
data.y2max = 5;

fig_index = fig_index + 1;
create_figure(data,fig_index,2)
save2pdf(strcat(path,data.fig_name,'.pdf'),fig_index,600)

%% figure // Current-Complex-ga
% Simulate using optimal ga
ga_index = find(results == max(results));
bs = 0.016; % m
```

```
ga = ga_index; % m
[t,x,Pout] = Simulation(bs,ga,2);

data.fig_name = 'Current_Complex_ga';
% label names
data.xname = '$t$ (s)';
data.yname = '$i$ (A)';
data.y1name = '$i_1$ (A)';
data.y2name = '$i_2$ (A)';
data.y3name = '$i_3$ (A)';
% state data
data.x1 = t;
data.y1 = x(:,3);   % current 1
data.y2 = x(:,4);   % current 2
data.y3 = x(:,5);   % current 3
% axis limits
data.xmin = 250;
data.xmax = 350;
data.ymin = -0.8*10^6;
data.ymax = 0.8*10^6;

fig_index = fig_index + 1;
create_figure(data,fig_index,3)
save2pdf(strcat(path,data.fig_name,'.pdf'),fig_index,600)

%% figure // Current_Complex_Zoom_ga
% Simulate using optimal ga
ga_index = find(results == max(results));
bs = 0.016; % m
ga = ga_index; % m
[t,x,Pout] = Simulation(bs,ga,2);

data.fig_name = 'Current_Complex_Zoom_ga';
% label names
data.xname = '$t$ (s)';
data.yname = '$i$ (A)';
data.y1name = '$i_1$ (A)';
data.y2name = '$i_2$ (A)';
data.y3name = '$i_3$ (A)';
% state data
data.x1 = t;
data.y1 = x(:,3);   % current 1
data.y2 = x(:,4);   % current 2
data.y3 = x(:,5);   % current 3
% axis limits
data.xmin = 255.2;
data.xmax = 267.8;
data.ymin = -0.8*10^6;
data.ymax = 0.8*10^6;

fig_index = fig_index + 1;
create_figure(data,fig_index,3)
save2pdf(strcat(path,data.fig_name,'.pdf'),fig_index,600)
```

B Appendix: Engineering Science Elements in this Report

This work presented in this report required learning several elements of engineering science deeply in order to successfully build, test and analyze a model of a wave energy converter generator.

The most significant aspect of engineering science that was studied here is electromagnetic theory. All relevant electromagnetic theories are detailed in the report. It is discussed in the first part of the report how a permanent magnet linear synchronous generator works, including the interaction between the translator and stator elements of the permanent magnet linear synchronous generator.

Another aspect of engineering science that was studied is the underlying principles of the incoming ocean waves. It is assumed in this report that the incoming ocean wave is sinusoidal, which is a significant simplification. The author is aware of polychromatic models of ocean waves that represent real waves more accurately. In addition, significant insights about the dynamics of the waves and wave energy converter were gained by constructing and testing both the simple and complex models. In the complex model it was assumed that the reaction force of the permanent magnet linear synchronous generator plays a part in the determination of the acceleration of the buoy. This was verified by showing the difference in simulation results between the simple and complex models.

Design issues were also investigated in this report, especially in the parametric studies section. A simple approach for design space exploration was used to investigate potential improvements in the system design. A series of parameter values were tested and plotted. Furthermore, constraints are considered so that the design is not without limits. Although the process is relatively simple, the idea of design was a core element of this project.

Finally, dynamic model stiffness was discussed, and tests were performed to evaluate model stiffness. Different MATLAB® solvers for differential equations were used to test the stiffness of the system based on time step evolution. The plots of the change of time-steps were analyzed, and it was concluded that the system is relatively stiff. This study demonstrates that a deeper understanding of numerical methods for engineering was developed, and is another significant aspect of engineering science that was learned during this project.